Supplementary Information

SI Section 1: Training Database

Table S1. Most of the data used in this study were not collected specifically for GEDI AGBD modeling. Each of the 142 projects represents a different number of sites, lidar instrument, plot size and shape. The site area is the total plot area per site. Several sites have multiple broad plant function type (PFT) classes as they span relatively large geographic scales or were collected in heterogeneous areas. Sites not included in the model fits presented in this paper are shaded grey. Datasets that are not included in the models either did not pass the data filtering criteria applied for this study, or were not available for the first set of models fit. The unused datasets are likely to be included in future versions of the GEDI L4A models, so this table can continue to be a useful reference for users of GEDI L4A data in the future. The four PFTs are Evergreen Broadleaf Trees (EBT), Evergreen Needleleaf Trees (ENT), Deciduous Broadleaf Trees (DBT) and Grassland Shrubland Woodland (GSW).

Country	***Site Name***	***N Plots***	***Site Area (ha)***	***Minimum tree diameter (cm)***	***Lidar Instrument***	***PFT***	***Allometric Model(s)***	***Co-Author Initials***	***Relevant Papers***
Australia	*AusPlots Forests*	*43*	*43*	*10*	*RIEGL LMS-Q560 and Leica ALS50-II*	*EBT, ENT*	*Paul et al. (2016)*	*A.G.Fisher*	*Wood et al. (2015)*
Australia	*TERN Supersites*	*8*	*8*	*10*	*RIEGL LMS-Q560 and Leica ALS60*	*EBT, GSW*	*Paul et al. (2016)*		
Australia	*JRSRP (Queensland)*	*38*	*11.9*		*RIEGL LMS-Q560 and RIEGL LMS-Q680i*	*EBT, GSW*	*Paul et al. (2016)*	*J. Armston*	
Australia	*ILCP*	*4*	*1*	*10*	*RIEGL LMS-Q560*	*DBT*	*Paul et al.(2016)*	*R.Lucas, J.Armston*	
Australia	*TERN Robson Creek*	*1*	*25*	*10*	*RIEGL LMS-Q560*	*EBT*	*Paul et al.(2016)*	*M. Bradford*	*Bradford et al. (2014)*

Australia	*SMAPEx*	*67*	*4.1*	*5*	*RIEGL LMS-Q560*	*GSW*	*Paul et al.(2016)*	*C. Rüdiger, M. Tanase, A. Monerris*	*Panciera et al. (2014)*
Brazil	*Fazenda Andiroba*	*40*	*7.65*	*35*	*Optech Orion*	*EBT*	*Chave et al. (2014)*	*M. Longo, M. Keller*	*Longo et al. (2016)*
Brazil	*Bonal*	*20*	*4.14*	*35*	*Optech Orion*	*EBT*	*Chave et al. (2014)*	*M. Longo, M. Keller*	*Longo et al. (2016)*
Brazil	*Fazenda Cauaxi*	*440*	*103.11*	*35*	*Optech ALTM 3100*	*EBT*	*Chave et al. (2014)*	*M. Longo, M. Keller*	*Longo et al. (2016)*
Brazil	*Feliz Natal*	*20*	*4.99*	*5*	*Optech Orion 09SEN243*	*EBT*	*Chave et al. (2014)*	*M. Longo, M. Keller*	*Longo et al. (2016)*
Brazil	*Floresta Nacional de Saraca-Taquera*	*40*	*9.5*	*35*	*Optech Orion*	*EBT*	*Chave et al. (2014)*	*M. Longo, M. Keller*	*Longo et al. (2016)*
Brazil	*Humaita*	*19*	*3.27*	*35*	*Optech Orion*	*EBT*	*Chave et al. (2014)*	*M. Longo, M. Keller*	*Longo et al. (2016)*
Brazil	*Floresta Nacional do Jamari*	*47*	*2.8*	*35*	*Optech Orion*	*EBT, DBT, GSW*	*Chave et al. (2014)*	*M. Longo, M. Keller*	*Longo et al. (2016)*
Brazil	*Sao Felix do Xingu*	*9*	*1.41*	*10*	*Optech ALTM 3100*	*EBT*	*Chave et al. (2014)*	*M. Longo, M. Keller*	*Longo et al. (2016)*
Brazil	*Sao Felix do Xingu*	*30*	*4.7*	*10*	*Optech ALTM 3100*	*EBT*	*Chave et al. (2014)*	*M. Longo, M. Keller*	*Longo et al. (2016)*
Brazil	*Tome-Acu*	*14*	*1.26*	*5*	*Optech Orion*	*EBT*	*Chave et al. (2014)*	*M. Longo, M. Keller*	*Longo et al. (2016)*
Brazil	*Talisma*	*10*	*2.09*	*35*	*Optech Orion*	*EBT*	*Chave et al. (2014)*	*M. Longo, M. Keller*	*Longo et al. (2016)*
Brazil	*Fazenda Tanguro*	*200*	*9.93*	*35*	*Optech ALTM 3100*	*EBT*	*Chave et al. (2014)*	*M. Longo, M. Keller*	*Longo et al. (2016)*
Canada	*Laurentides*	*30*	*1.2*	*NA*	*LVIS*	*DBT, ENT*	*NA*	*M. Simard*	*Simard & Denbina (2018)*
Canada	*Petawawa*	*249*	*15.56*	*9*	*RIEGL LMS-Q680i*	*DBT, ENT*	*Lambert et al. (2005)*	*J. White*	*White et al. (2019)*
China	*Cuilai*	*2*	*0.08*	*10*	*RIEGL LMS-Q280i*	*DBT*	*Forrester et al. (2017)*	*H. Huang*	
China	*Zhangye*	*3*	*0.19*	*3*	*RIEGL LMS-Q560*	*ENT*	*Forrester et al. (2017)*	*H. Huang*	

Colombia	*Choco*	*133*	*42.57*	*10*	*Optech ALTM 3033*	*EBT*	*Chave et al. (2014)*	*V. Meyer, S. Saatchi*	*Duque et al. (2017), Meyer et al. (2019)*
Costa Rica	*La Selva*	*3*	*2*	*5*	*Leica ALS50 and Optech 3100EA*	*EBT*	*Chave et al. (2014)*	*R. Chazdon*	*Dubayah et al. (2010), de Almeida (2020)*
Costa Rica	*La Selva*	*18*	*9*	*10*	*Leica ALS50 and Optech 3100EA*	*EBT*	*Chave et al. (2014)*	*D.B. Clark, D.A. Clark, J. Kellner*	*Clark, et al. (2011)*
Costa Rica	*Santa Rosa*	*12*	*12*	*5*	*LVIS*	*EBT*	*Chave et al. (2014)*	*A. Sanchez-Azofeifa, S. Calvo-Rodriguez.*	*Calvo-Rodriguez et al. (2021)*
Czech Republic	*Žofín*	*1*	*25.0*	*1*	*RIEGL VUX-1*	*DBT, ENT*	*Forrester et al. (2017)*	*J. Kellner, K. Kral, K.C. Cuschman, C. Zgraggen, B. Imbach, M. Krucek, T. Vrska, D. Janík*	*Kellner et al. (2019) Krůček et al. (2020) Janík et al. (2016)*
DRC	*Bastin*	*32*	*32*	*10*	*Optech ALTM 3100*	*EBT*	*Chave et al. (2014)*	*J.-F. Bastin*	*Bastin et al. (2014)*
DRC	*Kearsley*	*19*	*19*	*10*	*Optech ALTM 3100*	*EBT*	*Chave et al. (2014)*	*E. Kearsley, J. Bogaert, P. Boeckx*	*Kearsley et al. (2013)*
United Kingdom	*New Forest*	*41*	*3.69*	*10*	*Leica ALS50-II*	*DBT, ENT, EBT*	*Forrester et al. (2017)*	*R. Hill*	*Sumnall et al (2016)*
Estonia	*Järvselja (RAMI stands)*	*3*	*3*	*4*	*Leica ALS50-II*	*DBT, ENT*	*Forrester et al. (2017)*	*J. Pisek*	*Lang et al. (2017)*
French Guiana	*Paracou; Nouragues*	*25*	*151.5*	*10*	*RIEGL LMS-Q560 and RIEGL LMS-Q280i*	*EBT*	*Chave et al. (2014)*	*J. Chave*	*Labriere et al. (2018)*
Gabon	*Mabounie*	*21*	*21*	*10*	*RIEGL LMS-Q560*	*EBT*	*Chave et al. (2014)*	*N. Barbier*	*Labriere et al. (2018)*
Gabon	*Lope*	*12*	*10.5*	*5*	*RIEGL VQ-480i*	*EBT*	*Chave et al. (2014)*	*N. Labriere, S.L. Lewis*	*Labriere et al. (2018)*
Gabon	*Lope*	*13*	*1.04*	*10*	*RIEGL VQ-480i*	*EBT*	*Chave et al. (2014)*	*S.L. Lewis, K. Jeffery, L. White, K. Abernethy*	*Labriere et al. (2018)*

Gabon	*Mondah*	*15*	*15*	*1*	*RIEGL LMS-Q560*	*EBT*	*Chave et al. (2014)*	*J. Armston., L.E. Fatoyinbo Agueh, J. Poulsen, K. Jeffery, L. White*	*Fatoyinbo et al., in review*
Gabon	*Rabi*	*1*	*25*	*1*	*RIEGL VQ-480i*	*EBT*	*Chave et al. (2014)*	*H. Memiaghe, A. Alonso, D. Kenfack*	*Fatoyinbo et al., in review*
Germany	*Bavaria Forest*	*104*	*6.89*	*2*	*RIEGL Q-680i*	*ENT, DBT, GSW*	*Forrester et al. (2017)*	*A. Skidmore, M. Heurich*	*Krzystek et al. (2020), Latifi et al. (2015)*
Germany	*Tharandt*	*8*	*0.12*	*3.5*	*Leica ALS50-II*	*ENT*	*Forrester et al. (2017)*	*N. Kljun*	*Los et al. (2012)*
Germany	*Traunstein*	*1*	*24.91*	*5*	*RIEGL LMS-Q680i*	*DBT*	*Forrester et al. (2017)*	*A. Huth, N. Knapp, R. Fischer, K. Papathanassiou, H. Pretzsch, P. Biber*	*Knapp et al. (2020)*
Indonesia	*East Kalimantan*	*90*	*3.7*	*BAF 4.6 - 9.2 m^2/ha*	*Optech ALTM 3100*	*EBT*	*Chave et al. (2005)*	*P. Ellis*	*Ellis et al. (2016)*
Indonesia	*Mawas*	*16*	*1.6*	*5*	*Leica ALS80*	*EBT*	*Chave et al. (2014)*	*A. Ferraz, S. Saatchi*	*Ferraz et al. (2018)*
Indonesia	*Rmurezal*	*15*	*0.6*	*2*	*Leica ALS80*	*EBT*	*Chave et al. (2014)*	*A. Ferraz, S. Saatchi*	*Ferraz et al. (2018)*
Indonesia	*Rodamas*	*19*	*2.38*	*5*	*Leica ALS80*	*EBT*	*Chave et al. (2014)*	*A. Ferraz, S. Saatchi*	*Ferraz et al. (2018)*
Indonesia	*Sindolumber*	*12*	*3*	*5*	*Leica ALS80*	*EBT*	*Chave et al. (2014)*	*A. Ferraz, S. Saatchi*	*Ferraz et al. (2018)*
Indonesia	*Sumalindo*	*12*	*3*	*10*	*Leica ALS80*	*EBT*	*Chave et al. (2014)*	*A. Ferraz, S. Saatchi*	*Ferraz et al. (2018)*
Indonesia	*Timberdana*	*11*	*1.38*	*5*	*Leica ALS80*	*EBT*	*Chave et al. (2014)*	*A. Ferraz, S. Saatchi*	*Ferraz et al. (2018)*
Indonesia	*Tuanam*	*6*	*0.54*	*5*	*Leica ALS80*	*EBT*	*Chave et al. (2014)*	*A. Ferraz, S. Saatchi*	*Ferraz et al. (2018)*

Indonesia	*USFS*	*6*	*6*	*5*	*Leica ALS80*	*EBT*	*Chave et al. (2014)*	*A. Ferraz, S. Saatchi*	*Ferraz et al. (2018)*
Italy	*Sella*	*1*	*4.84*	*1*	*Optech ALTM 3100*	*ENT*	*Forrester et al. (2017)*	*C. Torreson, P. Corona*	*Corona et al. (2014)*
Italy	*Trentino*	*152*	*16.32*	*3*	*Optech ALTM 3100EA*	*ENT, DBT*	*Forrester et al. (2017)*	*M. Dalponte*	*Dalponte and Coomes (2016)*
Japan	*Nagano*	*2*	*2.2*	*5*	*Leica ALS70-HP*	*ENT*	*NA*	*S. Deng, M. Katoh*	*Deng et al. (2016)*
Malaysia	*Selangor*	*54*	*2.6*	*1*	*Leica ALS50-II*	*EBT*	*Chave et al. (2014)*	*D. Boyd, P. Aplin*	*Brown et al. (2018)*
Malaysia	*Danum Valley*	*1*	*50*	*1*	*Leica ALS50-II*	*EBT*	*Chave et al. (2014)*	*D. Coomes, D. Burslem, M. Cutler, M. O'Brien*	*Philipson et al. (2020)*
Malaysia	*Sepilok*	*9*	*36*	*1*	*Leica ALS50-II*	*EBT*	*Chave et al. (2014)*	*D. Coomes, D.Burslem*	*Jucker et al. (2018)*
Mexico	*NFI*	*351*	*351*	*7.5*	*RIEGL VQ-480*	*EBT, DBT, ENT, GSW*	*NA*	*J. Fernandez*	
Netherlands	*Loobos*	*8*	*0.12*	*16*	*Leica ALS50-II*	*ENT*	*Muukkonen (2007)*	*N. Kljun*	*Los et al. (2012)*
New Zealand	*Forest Service*	*154*	*9.24*	*2.5*	*Optech Orion M200*	*EBT, ENT, DBT, GSW*	*Moore (2010), Beets et al. (2012)*	*J. Dash*	
Panama	*Barro Colorado Island*	*1*	*50*	*1*	*Optech Gemini*	*EBT*	*Chave et al. (2014)*	*J. Kellner, R. Condit, S. Hubbell, J. Dalling*	*Condit et al. (2020, 2019) Lobo & Dalling (2014)*
Peru	*Tambopata*	*6*	*6*	*10*	*Leica ALS50-II*	*EBT*	*Chave et al. (2014)*	*R. Hill, O. Phillips, D. Boyd, T. Baker, C. Hopkinson, R. Vásquez Martínez, A. Monteagdo Mendoza*	*Boyd et al. (2013)*
Poland	*Bialowieza*	*343*	*17.15*	*7*	*RIEGL LMS-Q680i*	*ENT, DBT*	*Forrester et al. (2017)*	*K. Stereńczak*	*Stereńczak et al. (2019, 2017)*

South Africa	*Agincourt; D'Nyala; Ireagh; Justicia; Venetia; Welverdiend*	*20*	*20*	*3*	*Optech Gemini and Optech ALTM 3100*	*GSW, DBT*	*Colgan et al. (2013)*	*L.Naidoo, R. Main, R. Mathieu, K. Wessels, B.Erasmus, R.J.Scholes*	*Naidoo et al. (2015)*
Spain	*Monfragüe*	*7*	*0.49*	*7.5*	*Leica ALS50*	*ENT, GSW*	*Forrester et al. (2017)*	*S. de Miguel., A. Fernandez-Landa*	*Fernández-Landa (2015)*
Spain	*Soria*	*43*	*2.15*	*10*	*Leica ALS60-II*	*GSW, ENT*	*Forrester et al. (2017)*	*S. de Miguel., A. Fernandez-Landa*	*Fernández-Landa (2015)*
Spain	*Soria*	*1*	*1*	*10*	*Leica ALS60-II*	*ENT*	*Forrester et al. (2017)*	*S. de Miguel., A. Fernandez-Landa*	*Fernández-Landa (2015)*
Spain	*Valsain circle plots*	*25*	*3.14*	*10*	*Leica ALS50-II*	*ENT*	*Forrester et al. (2017)*	*R. Valbuena, J.A. Manzanera, A. Garcia-Abril*	*Valbuena et al. (2012; 2013)*
Spain	*Valsain*	*54*	*2.86*	*7.5*	*Leica ALS50*	*ENT, GSW*	*Forrester et al. (2017)*	*S. de Miguel., A. Fernandez-Landa*	*Fernández-Landa (2015)*
Spain	*Valsain rectangular plots*	*6*	*1.44*	*0*	*Leica ALS50-II*	*ENT*	*Forrester et al. (2017)*	*R. Valbuena, J.A. Manzanera, A. Garcia-Abril*	*Valbuena et al. (2012; 2013)*
Switzerland	*Laegeren*	*1*	*4.81*	*20*	*RIEGL LMS-Q680i*	*DBT*	*Forrester et al. (2017)*	*F. Morsdorf*	*Schneider et al. (2017) Kükenbrink et al. (2017)*
Tanzania	*Amani*	*153*	*15.3*	*10*	*Leica ALS70*	*EBT*	*Masota et al. (2016)*	*E. Næsset, T. Gobakken., E. Zahabu*	*Hansen et al. (2015)*
Tanzania	*Liwale*	*513*	*36.26*	*1*	*Leica ALS70*	*DBT, EBT, GSW*	*Mugasha et al. (2013)*	*E. Næsset, T. Gobakken., E. Zahabu*	*Ene et al. (2017)*
USA	*Cascade East Zone, Washington*	*40*	*1.62*	*0.5*	*Leica ALS50-II*	*GSW, ENT*	*Jenkins et al. (2003)*	*A. Hudak, M. Falkowski., P. Fekety*	*Fekety et al. (2020)*

USA	*CFLRA, Idaho*	*41*	*1.66*	*0.5*	*Leica ALS50-II, Leica ALS60, Leica ALS70, and Optech Gemini*	*ENT, GSW, DBT*	*Jenkins et al. (2003)*	*A. Hudak, M. Falkowski., P. Fekety*	*Fekety et al. (2020)*
USA	*Clear Creek, Idaho*	*53*	*2.14*	*0.5*	*Leica ALS60*	*ENT*	*Jenkins et al. (2003)*	*A. Hudak, M. Falkowski., P. Fekety*	*Fekety et al. (2020)*
USA	*Clear Creek, Idaho; Selway, Idaho*	*42*	*2.06*	*10*	*Leica ALS60*	*ENT*	*Jenkins et al. (2003)*	*L. Boschetti, N. Sanchez-Lopez*	*Sanchez-Lopez et al. (2020a, 2020b)*
USA	*Colorado*	*46*	*3.75*	*2.5*	*RIEGL LMS-Q680i*	*GSW, ENT, DBT*	*Jenkins et al. (2003)*	*H. Andersen, W. Cohen*	*Legner et al., (2020)*
USA	*Colville, Washington*	*111*	*8.98*	*0.5*	*Leica ALS50, Leica ALS60, Leica ALS70 HP*	*ENT*	*Jenkins et al. (2003)*	*A. Hudak, M. Falkowski., P. Fekety*	*Fekety et al. (2020)*
USA	*Damon, Oregon*	*98*	*3.97*	*0.5*	*Leica ALS50-II*	*ENT, GSW*	*Jenkins et al. (2003)*	*A. Hudak, M. Falkowski., P. Fekety*	*Fekety et al. (2020)*
USA	*DCEF, Idaho*	*73*	*1.23*	*2.5*	*Leica ALS50-II*	*ENT*	*Jenkins et al. (2003)*	*A. Hudak, M. Falkowski., P. Fekety*	*Fekety et al. (2020)*
USA	*Michigan*	*333*	*13.48*	*NA*	*RIEGL LMS-Q680i*	*DBT, GSW, ENT*	*Jenkins et al. (2003)*	*M. Falkowski*	*Falkowski, unpublished data*
USA	*Fernan, Idaho*	*34*	*1.38*	*1.3*	*Leica ALS40, Leica ALS50-II*	*ENT*	*Jenkins et al. (2003)*	*A. Hudak, M. Falkowski., P. Fekety*	*Fekety et al. (2020)*
USA	*Fitsum, Idaho*	*20*	*0.81*	*12.7*	*Leica ALS50-II*	*ENT, GSW*	*Jenkins et al. (2003)*	*A. Hudak, M. Falkowski., P. Fekety*	*Hudak, unpublished data*
USA	*Harvard Forest, Massachusetts*	*1*	*35*	*1*	*Optech ALTM Gemini*	*DBT*	*Jenkins et al. (2003)*	*D. Orwig, P. Boucher*	*Orwig et al. (2015, n.d.)*
USA	*Maine*	*48*	*3.92*	*2.5*	*RIEGL LMS-Q680i*	*DBT, ENT*	*Jenkins et al. (2003)*	*H. Andersen, W. Cohen*	*Legner et al., (2020)*
USA	*Minnesota*	*50*	*4.08*	*2.5*	*RIEGL LMS-Q680i*	*DBT, ENT*	*Jenkins et al. (2003)*	*H. Andersen, W. Cohen*	*Legner et al., (2020)*
USA	*Moscow Mtn, Idaho*	*173*	*7*	*10.2*	*Leica ALS40, Leica ALS50-II, NA*	*ENT, GSW*	*Jenkins et al. (2003)*	*A. Hudak, M. Falkowski., P. Fekety*	*Fekety et al. (2020)*
USA	*NEON ABBY, Washington*	*27*	*1.64*	*10*	*Optech ALTM Gemini*	*ENT*	*Jenkins et al. (2003)*		*Krause and Goulden (2015), Meier*

									and Jones (2020)
USA	*NEON BART, New Hampshire*	*40*	*2.4*	*10*	*Optech ALTM Gemini*	*DBT*	*Jenkins et al. (2003)*		*Krause and Goulden (2015), Meier and Jones (2020)*
USA	*NEON BLAN, Virginia*	*24*	*0.96*	*10*	*Optech ALTM Gemini*	*DBT*	*Jenkins et al. (2003)*		*Krause and Goulden (2015), Meier and Jones (2020)*
USA	*NEON CLBJ, Texas*	*43*	*1.72*	*10*	*Optech ALTM Gemini*	*DBT, GSW*	*Jenkins et al. (2003)*		*Krause and Goulden (2015), Meier and Jones (2020)*
USA	*NEON CPER, Colorado*	*50*	*2.0*	*10*	*Optech ALTM Gemini*	*GSW*	*Jenkins et al. (2003)*		*Krause and Goulden (2015), Meier and Jones (2020)*
USA	*NEON DELA, Alabama*	*21*	*1.64*	*10*	*Optech ALTM Gemini*	*DBT*	*Jenkins et al. (2003)*		*Krause and Goulden (2015), Meier and Jones (2020)*
USA	*NEON DSNY, Florida*	*19*	*0.76*	*10*	*Optech ALTM Gemini*	*ENT, EBT*	*Jenkins et al. (2003)*		*Krause and Goulden (2015), Meier and Jones (2020)*
USA	*NEON GRSM, Tennessee*	*40*	*2.4*	*10*	*Optech ALTM Gemini*	*DBT, ENT*	*Jenkins et al. (2003)*		*Krause and Goulden (2015), Meier and Jones (2020)*
USA	*NEON GUAN, Puerto Rico*	*38*	*2.28*	*10*	*Optech ALTM Gemini*	*EBT*	*Jenkins et al. (2003)*		*Krause and Goulden (2015), Meier and Jones (2020)*
USA	*NEON HARV, Massachusetts*	*39*	*2.36*	*10*	*Optech ALTM Gemini*	*DBT, ENT*	*Jenkins et al. (2003)*		*Krause and Goulden (2015), Meier and Jones (2020)*
USA	*NEON JERC, Georgia*	*21*	*1.64*	*10*	*Optech ALTM Gemini*	*DBT*	*Jenkins et al. (2003)*		*Krause and Goulden*

									(2015), Meier and Jones (2020)
USA	*NEON JORN, New Mexico*	*50*	*2.0*	*10*	*Optech ALTM Gemini*	*GSW*	*Jenkins et al. (2003)*		*Krause and Goulden (2015), Meier and Jones (2020)*
USA	*NEON KONZ, Kansas*	*13*	*0.52*	*10*	*Optech ALTM Gemini*	*GSW*	*Jenkins et al. (2003)*		*Krause and Goulden (2015), Meier and Jones (2020)*
USA	*NEON LAJA, Puerto Rico*	*4*	*0.16*	*10*	*Optech ALTM Gemini*	*EBT*	*Jenkins et al. (2003)*		*Krause and Goulden (2015), Meier and Jones (2020)*
USA	*NEON LENO, Alabama*	*13*	*0.52*	*10*	*Optech ALTM Gemini*	*DBT*	*Jenkins et al. (2003)*		*Krause and Goulden (2015), Meier and Jones (2020)*
USA	*NEON MLBS, Virginia*	*4*	*0.16*	*10*	*Optech ALTM Gemini*	*DBT, ENT*	*Jenkins et al. (2003)*		*Krause and Goulden (2015), Meier and Jones (2020)*
USA	*NEON MOAB, Utah*	*50*	*2*	*10*	*Optech ALTM Gemini*	*GSW, ENT*	*Jenkins et al. (2003)*		*Krause and Goulden (2015), Meier and Jones (2020)*
USA	*NEON NIWO, Colorado*	*28*	*1.12*	*10*	*Optech ALTM Gemini*	*ENT, GSW*	*Jenkins et al. (2003)*		*Krause and Goulden (2015), Meier and Jones (2020)*
USA	*NEON NOGP, North Dakota*	*29*	*1.16*	*10*	*Optech ALTM Gemini*	*GSW*	*Jenkins et al. (2003)*		*Krause and Goulden (2015), Meier and Jones (2020)*
USA	*NEON ONAQ, Utah*	*50*	*2.0*	*10*	*Optech ALTM Gemini*	*GSW, ENT*	*Jenkins et al. (2003)*		*Krause and Goulden (2015), Meier and Jones (2020)*

USA	*NEON ORNL, Tennessee*	*37*	*2.28*	*10*	*Optech ALTM Gemini*	*DBT, ENT*	*Jenkins et al. (2003)*		*Krause and Goulden (2015), Meier and Jones (2020)*
USA	*NEON OSBS, Florida*	*42*	*2.48*	*10*	*Optech ALTM Gemini*	*EBT, DBT*	*Jenkins et al. (2003)*		*Krause and Goulden (2015), Meier and Jones (2020)*
USA	*NEON PUUM, Hawaii*	*21*	*0.84*	*10*	*Optech ALTM Gemini*	*EBT*	*Jenkins et al. (2003)*		*Krause and Goulden (2015), Meier and Jones (2020)*
USA	*NEON RMNP, Colorado*	*29*	*1.52*	*10*	*Optech ALTM Gemini*	*ENT, DBT*	*Jenkins et al. (2003)*		*Krause and Goulden (2015), Meier and Jones (2020)*
USA	*NEON SCBI, Virginia*	*35*	*2.2*	*10*	*Optech ALTM Gemini*	*DBT*	*Jenkins et al. (2003)*		*Krause and Goulden (2015), Meier and Jones (2020)*
USA	*NEON SERC, Maryland*	*39*	*2.4*	*10*	*Optech ALTM Gemini*	*DBT, GSW*	*Jenkins et al. (2003)*		*Krause and Goulden (2015), Meier and Jones (2020)*
USA	*NEON SJER, California*	*28*	*1.92*	*10*	*Optech ALTM Gemini*	*DBT, ENT*	*Jenkins et al. (2003)*		*Krause and Goulden (2015), Meier and Jones (2020)*
USA	*NEON SOAP, California*	*21*	*1.64*	*10*	*Optech ALTM Gemini*	*ENT, DBT*	*Jenkins et al. (2003)*		*Krause and Goulden (2015), Meier and Jones (2020)*
USA	*NEON SRER, Arizona*	*23*	*1.64*	*10*	*Optech ALTM Gemini*	*GSW*	*Jenkins et al. (2003)*		*Krause and Goulden (2015), Meier and Jones (2020)*
USA	*NEON STEI, Wisconsin*	*37*	*2.16*	*10*	*Optech ALTM Gemini*	*DBT, ENT*	*Jenkins et al. (2003)*		*Krause and Goulden (2015), Meier and Jones (2020)*

USA	*NEON TALL, Alabama*	*40*	*2.4*	*10*	*Optech ALTM Gemini*	*DBT*	*Jenkins et al. (2003)*		*Krause and Goulden (2015), Meier and Jones (2020)*
USA	*NEON TEAK, California*	*20*	*1.6*	*10*	*Optech ALTM Gemini*	*ENT*	*Jenkins et al. (2003)*		*Krause and Goulden (2015), Meier and Jones (2020)*
USA	*NEON TREE, Wisconsin*	*40*	*2.4*	*10*	*Optech ALTM Gemini*	*ENT, DBT, DNT*	*Jenkins et al. (2003)*		*Krause and Goulden (2015), Meier and Jones (2020)*
USA	*NEON UKFS, Kansas*	*37*	*2.28*	*10*	*Optech ALTM Gemini*	*DBT, ENT*	*Jenkins et al. (2003)*		*Krause and Goulden (2015), Meier and Jones (2020)*
USA	*NEON UNDE, Michigan*	*20*	*1.6*	*10*	*Optech ALTM Gemini*	*DBT, ENT*	*Jenkins et al. (2003)*		*Krause and Goulden (2015), Meier and Jones (2020)*
USA	*NEON WOOD, North Dakota*	*36*	*1.44*	*10*	*Optech ALTM Gemini*	*GSW*	*Jenkins et al. (2003)*		*Krause and Goulden (2015), Meier and Jones (2020)*
USA	*NEON WREF, Washington*	*20*	*1.6*	*10*	*Optech ALTM Gemini*	*ENT*	*Jenkins et al. (2003)*		*Krause and Goulden (2015), Meier and Jones (2020)*
USA	*NEON YELL, Wyoming*	*17*	*0.68*	*10*	*Optech ALTM Gemini*	*GSW, ENT*	*Jenkins et al. (2003)*		*Krause and Goulden (2015), Meier and Jones (2020)*
USA	*New England*	*57*	*57*	*10*	*RIEGL VQ-480*	*DBT, ENT*	*Jenkins et al. (2003)*	*P. Montesano*	*Huang et al. (2013) Montesano et al. (2013)*
USA	*Nez Perce, Idaho*	*112*	*9.06*	*1.3*	*Leica ALS40*	*ENT, GSW*	*Jenkins et al. (2003)*	*A. Hudak, M. Falkowski., P. Fekety*	*Jensen et al. (2008)*
USA	*Oregon*	*50*	*4.08*	*2.5*	*RIEGL LMS-Q680i*	*ENT, GSW*	*Jenkins et al. (2003)*	*H. Andersen, W. Cohen*	*Legner et al., (2020)*

USA	*Pennsylvania; New Jersey*	*49*	*4*	*2.5*	*RIEGL LMS-Q680i*	*DBT, ENT, GSW*	*Jenkins et al. (2003)*	*H. Andersen, W. Cohen*	*Legner et al., (2020)*
USA	*PREF, Idaho*	*96*	*3.88*	*2.5*	*Leica ALS50-II*	*ENT*	*Jenkins et al. (2003)*	*A. Hudak, M. Falkowski., P. Fekety*	*Fekety et al. (2020)*
USA	*PREF, Idaho*	*60*	*67.58*	*2.5*	*Leica ALS50-II*	*ENT*	*Jenkins et al. (2003)*	*A. Hudak, M. Falkowski., P. Fekety*	*Fekety et al. (2020)*
USA	*South Carolina*	*50*	*4.08*	*2.5*	*RIEGL LMS-Q680i*	*DBT, ENT, EBT*	*Jenkins et al. (2003)*	*H. Andersen, W. Cohen*	*Legner et al., (2020)*
USA	*SERC, Maryland*	*1*	*16*	*1*	*RIEGL VQ-480*	*DBT*	*Jenkins et al. (2003)*	*G. Parker*	*Duncanson et al., (2015)*
USA	*Teakettle*	*12*	*12*	*10*	*Optech Gemini*	*ENT*	*Jenkins et al. (2003)*	*R. Dubayah*	*Duncanson et al., (2015)*
USA	*Slate Creek, Idaho*	*90*	*3.64*	*0.5*	*Leica ALS50*	*ENT, GSW*	*Jenkins et al. (2003)*	*A. Hudak, M. Falkowski., P. Fekety*	*Fekety et al. (2020)*
USA	*Sonoma County, California*	*154*	*4.88*	*BAF 1.5 - 6.8 m^2/ha*	*Leica ALS50 and ALS70*	*ENT, EBT, DBT, GSW*	*Jenkins et al. (2003)*	*L. Duncanson*	*Dubayah et al., (2017) Duncanson et al., (2017)*
USA	*Sonoma County, California*	*13*	*0.64*	*4*	*Leica ALS50 and ALS70*	*DBT, ENT*	*Jenkins et al. (2003)*	*L. Duncanson*	*Duncanson et al., (2020)*
USA	*Sonoma County, California*	*13*	*0.54*	*BAF 1.5 - 6.8 m^2/ha*	*Leica ALS50 and ALS70*	*DBT, ENT*	*Jenkins et al. (2003)*	*L. Duncanson*	*Duncanson et al., (2020)*
USA	*Sonoma County, California*	*19*	*1.24*	*BAF 1.5 - 6.8 m^2/ha*	*Leica ALS50 and ALS70*	*ENT, EBT*	*Jenkins et al. (2003)*	*L. Duncanson*	*Duncanson et al., (2020)*
USA	*Stanley, Idaho*	*27*	*1.09*	*7*	*Leica ALS50-II*	*ENT, GSW*	*Jenkins et al. (2003)*	*A. Hudak, M. Falkowski., P. Fekety*	*Fekety et al. (2020)*
USA	*St. Joe, Idaho*	*79*	*6.37*	*1.3*	*Leica ALS40*	*ENT*	*Jenkins et al. (2003)*	*A. Hudak, M. Falkowski., P. Fekety*	*Fekety et al. (2020)*
USA	*Tepee Creek, Idaho*	*39*	*1.58*	*0.5*	*Leica ALS50-II*	*ENT*	*Jenkins et al. (2003)*	*A. Hudak, M. Falkowski., P. Fekety*	*Fekety et al. (2020)*

USA	*Upper Lolo, Idaho*	*26*	*1.05*	*0.5*	*Leica ALS50*	*ENT*	*Jenkins et al. (2003)*	*A. Hudak, M. Falkowski., P. Fekety*	*Fekety et al. (2020)*

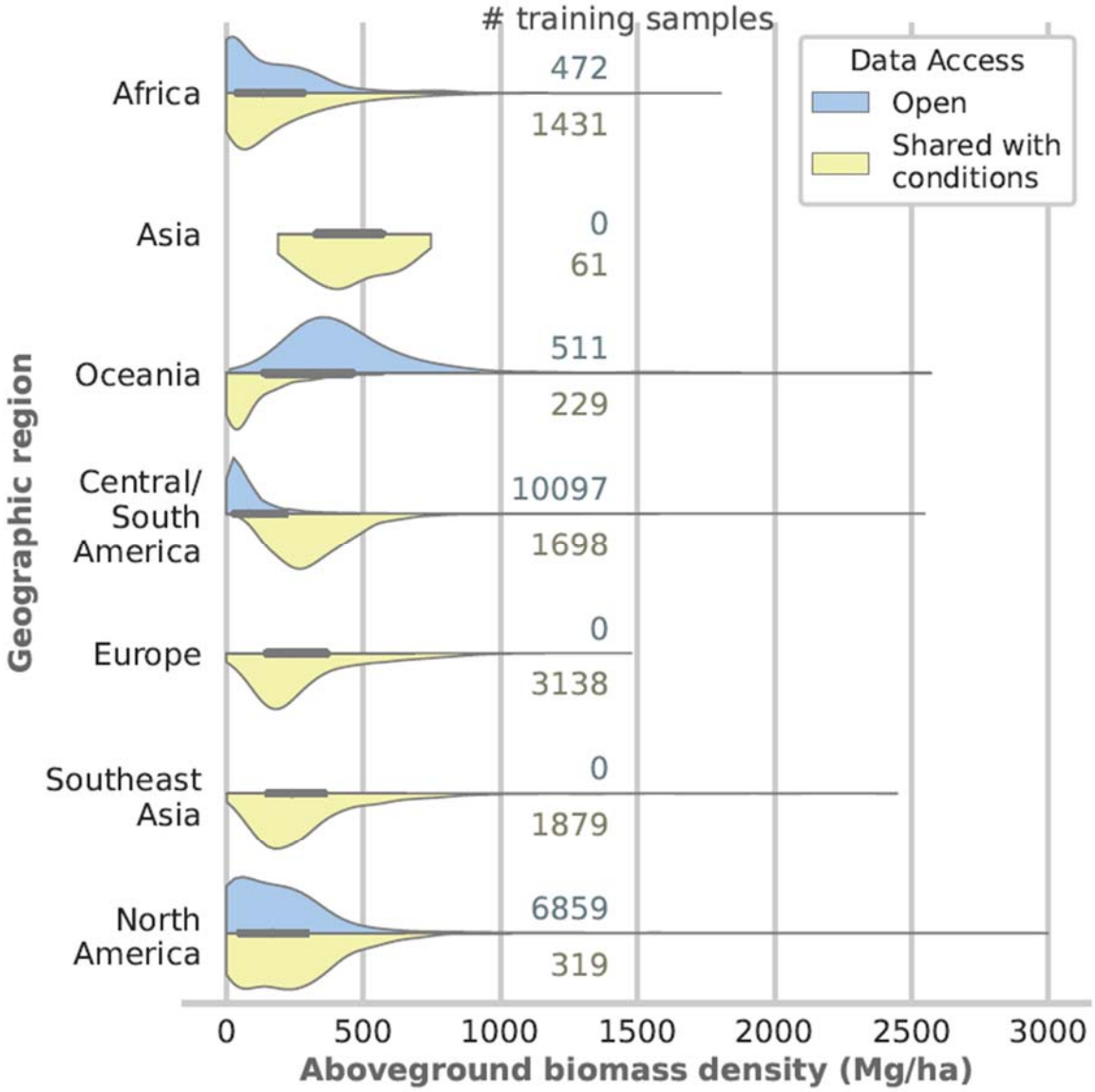

Fig. S1 shows the distributions of open and conditionally shared data in the GEDI Forest Structure and Biomass Database (FSBD) per continent. Note this represents the full database at the time of publication including all sites listed in Table S1. Not all of this data is included

in the models presented in this paper, as described in the methods section on data filtering. Some datasets were also not included due to incomplete metadata at the time of model fitting, and will be considered for future versions of GEDI04_A. The AGBD here is for GEDI footprint-sized plots (~25 m diameter circle).

Database Filtering Prior to AGBD Model Fitting

Models are only as good as the data that train them, and this is true for GEDI04_A algorithms. We used a uniquely heterogeneous database, collating and curating data from many disparate sources. While many of the input datasets were well geolocated (<5 m), in many cases a lack of correlation between lidar and field datasets suggested that one or both had either spatial or temporal mismatches. Of all the iterative processing analyses conducted through the development of these models, refinements and filtering of the input datasets routinely yielded the largest improvements. Indeed, our particular application of a filter between field and lidar estimated maximum height yielded the most substantial increase in model performance.

The first filter was based on a comparison of the maximum measured or modeled (using a local height-diameter model) tree height in each GEDI footprint-sized field plot to the lidar-estimated maximum height. In this case we used RH98 instead of RH100 because RH100 has been demonstrated to be sensitive to noise. When AGBD was < 1 Mg/ha and RH98 was > 5 m, the footprint was excluded, assuming that there was either a geolocation mismatch or the field survey did not measure small trees (e.g. DBH <10 cm). Similarly, when AGBD was > 150 Mg/ha and RH98 < 5 m, the footprint was excluded, in this case presuming a geolocation mismatch. Third, if there is more than 10 m difference between field measured or modeled

maximum tree height and lidar-estimated tree height, these footprints were excluded. See Fig S2 for an assessment of sensitivity in this height difference filter on the percentage of data removed from the training dataset. These filters accounted for a) poor geolocation of the field data, b) temporal changes between the field and lidar collection, c) measurement or transcription error in the field data, or d) in the case of modeled heights, an inappropriate diameter to height allometric model. Finally, to minimize allometric model error, we filtered plots including trees outside the calibration range of the applied allometric model. The models of Jenkins (2003), for example, were developed using field measurements of evergreen needleleaf trees in North America with a maximum DBH of 2.5 m. We therefore excluded simulated footprints that contained at least one tree with a DBH greater than this value.

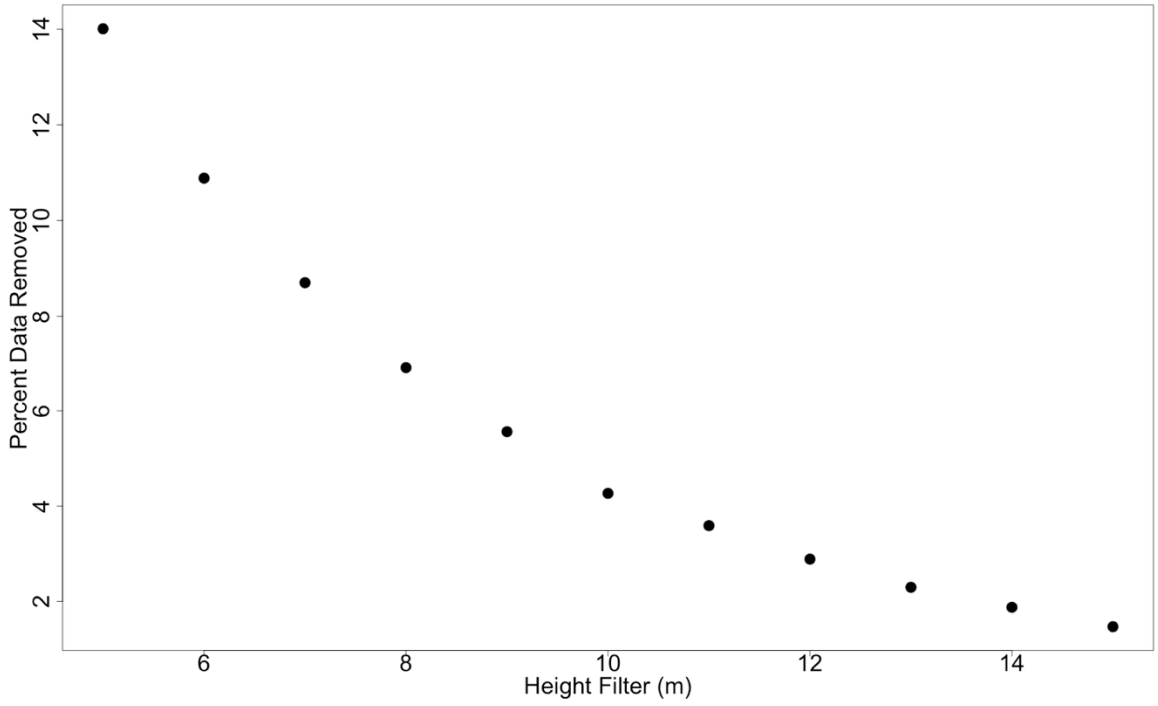

Fig. S2 The percentage of data removed prior to AGBD model fitting based on the height filter between plot-level maximum height (RH98) and field estimated maximum height. A 10 m difference was selected as the filter for GEDI04_A.

SI Section 2: Results from alternative model stratification and candidate predictor sets

Table S2. Top model statistics for model fits considering all candidate predictors. This differs from Table 2, where models were forced to include RH98, and could not include metrics lower than RH50.

Strata	R^2	%Rmse	MRE (Mg/ha)	Transform	Predictors
DBT Africa	0.6	56.12	5.99	sqrt-sqrt	RH10, RH30xRH40, RH30xRH80
DBT Europe	0.39	48.86	3.84	original-log	RH10xRH50, RH20xRH98, RH50xRH98
DBT North America	0.6	35.05	7.6	sqrt-sqrt	RH20xRH30, RH20xRH80
EBT Africa	0.75	68.02	11.31	sqrt-sqrt	RH80
EBT Asia	0.53	60.31	75.75	sqrt-sqrt	RH20
EBT Oceania	0.61	28.66	8.17	sqrt-sqrt	RH70, RH98
EBT South America	0.62	41.66	5.56	sqrt-sqrt	RH80, RH10xRH60
ENT Oceania	0.57	58.06	11.21	sqrt-sqrt	RH40xRH98
ENT Europe	0.67	35.72	11.77	original-sqrt	RH10xRH_80, RH20xRH40, RH50xRH60

ENT North America	0.62	65.37	9.77	sqrt-sqrt	RH90, RH10xRH80
GSW Oceania	0.8	36.84	2.93	original-sqrt	RH20, RH60xRH98

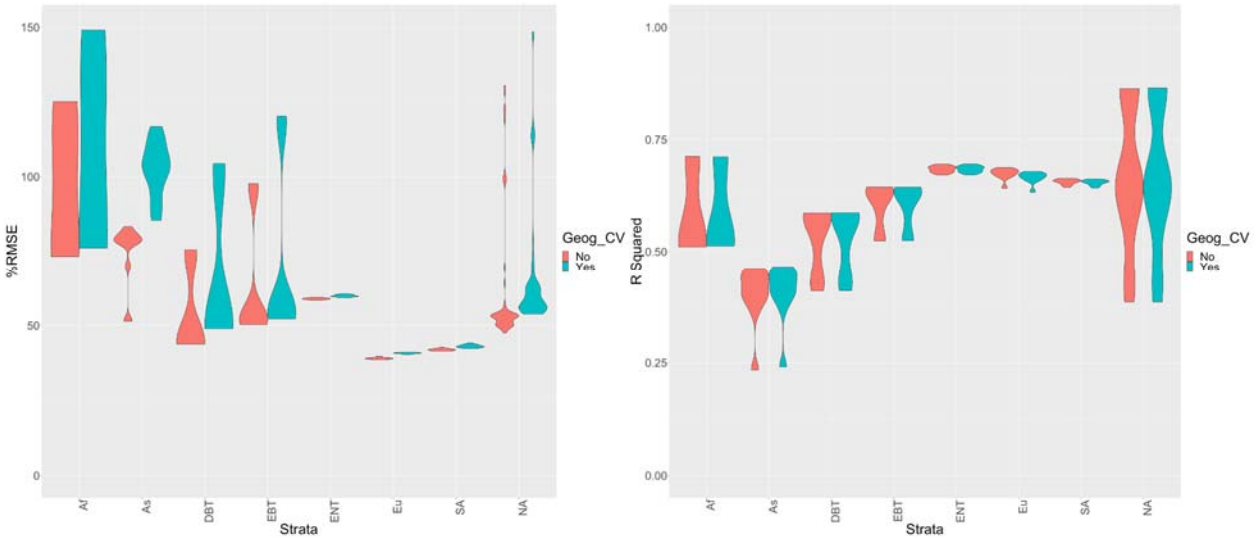

Fig. S3. Comparison of results when calculating %RMSE and R^2 on model fits with and without geographic cross validation (Geog_CV) at the broadly stratified PFT, and geographic region for the constrained models.

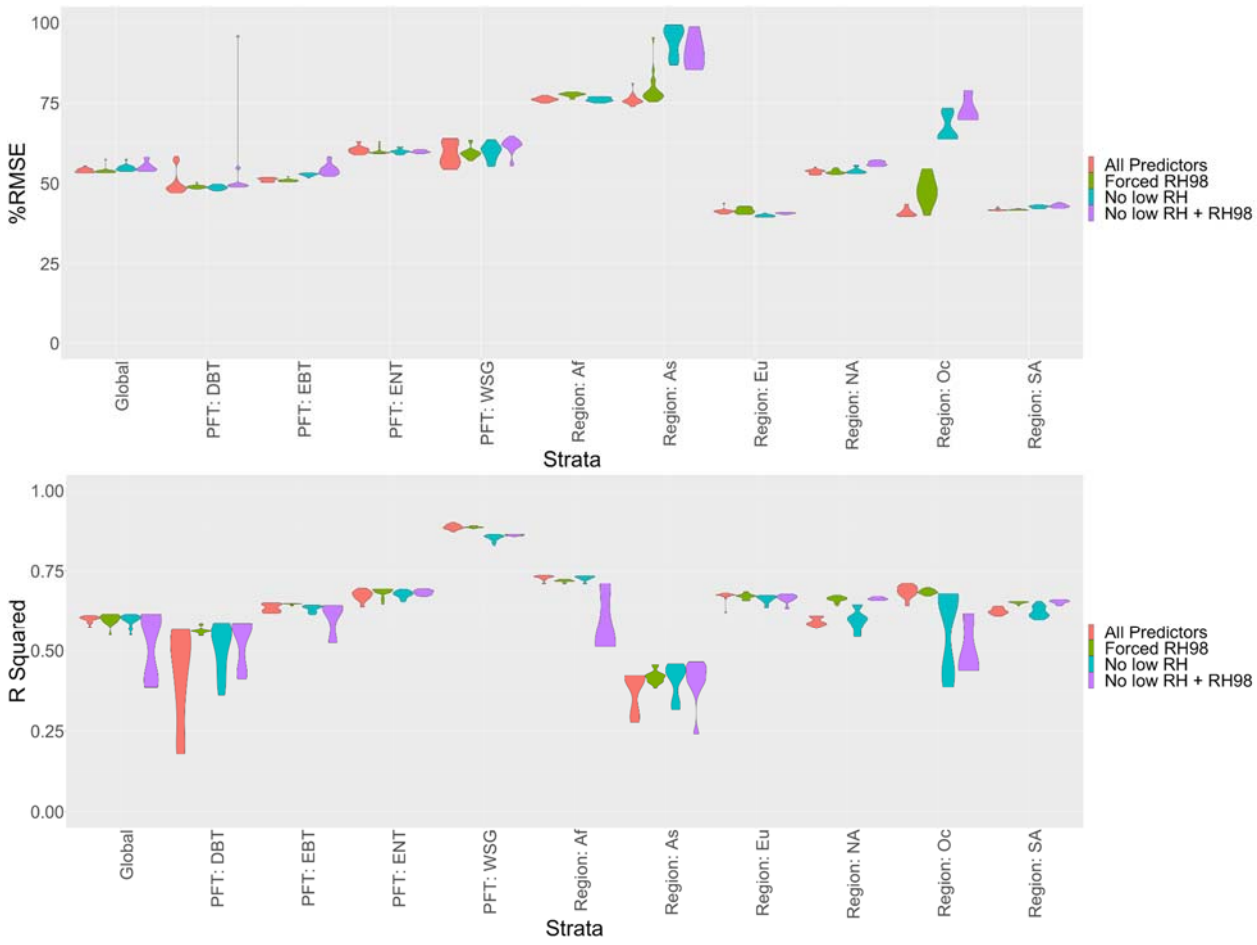

Fig. S4. Comparison of results from four different model fitting scenarios fit at a broad strata, either by PFT, geographic region, or globally. Models are assessed by geographic cross validation.

SI Section 3: Alternative model fitting approaches

Comparison of OLS to other Model Forms

To determine whether predictive capability was lost by adopting parametric models, several other popularly employed empirical AGBD modeling techniques were explored, including machine learning approaches. This exploration was justified for each of these approaches below, highlighting the theoretical or practical advantages of each approach. Note that typically machine

learning approaches require more representative training samples and thus may not be as well suited or transferable to the opportunistic samples available in the GEDI Forest Structure and Biomass Database (Demaerschalk and Kozak, 1974).

PLS

Partial Least Squares (PLS) regression is a technique for empirical modeling that allows for the inclusion of multiple highly correlated predictor variables in the statistical framework of parametric regression (Abdi, 2010). Similar to Canonical Correlation Analysis (e.g. Valbuena et al. 2012), PLS recombines a suite of input variables into new, uncorrelated predictors through application of a series of weights between the original and new predictors. In this example, the full suite of RH metrics and interaction terms could be used for predicting AGBD regardless of high variable correlations. The weightings on the original variables also enable an appreciation of which original predictors are more important for AGBD prediction, unlike more black-box algorithms such as Support Vector Machines. The PLS algorithm used in this comparison was the one implemented in the plsr package in R (Mevik and Wehrens, 2007).

Random Forests models

Random Forests algorithms have become popularly used in a wide range of remote sensing applications, often for producing spatially-explicit maps when the relationship between the mapped variable and predictor variables is unknown, nonlinear, or the predictor variables are not numeric. Random Forests are an extension of the Classification And Regression Tree (CART) algorithm (Breiman, 2001). The R package randomForest was used for model fitting. A forest is a user-determined number of decision trees (*ntree*), where each decision tree is grown by

randomly sampling approximately two thirds of the training data with replacement. At each node of each tree, *mtry* variables are randomly selected from the set of predictors (in this case RH metrics and interaction terms). The best split using these *n (mtry/3)* variables is at the split point for the predictor that results in the greatest reduction in residual sums of squares between the sample of observations and the node mean. This process is used to perform recursive binary splits of the data. The value of *mtry* is held constant and each decision tree is grown to the largest extent possible (with no pruning). This process is repeated to build an ensemble of regression trees, where each tree (for the continuous variables used here) is a regression model that exhibits low mean residual error, but a large variance. The predictions are then averaged to calculate a final estimate of the response variable. For our Random Forest fits we used a *mtry* of 18 (total number of predictors divided by 3) and *ntree* of 500, respectively.

Support Vector Regression

Support Vector Regression is an extension of the classification-focused Support Vector Machines (SVM) that, similarly to Random Forests, have become popular for developing nonlinear predictive relationships between a suite of input predictors and a response variable. SVM finds the least complex function where a deviation from the response variable (i.e., AGBD) is less than the variance in the training dataset by developing a series of support vectors from some subset of the training data, and testing their efficacy for classification or in this case regression on the remaining training data (Drucker et al., 1996). SVM was implemented in R using the package svm (Meyer, 2020). Note that for implementation of the machine learning techniques (SVM and RF), common but default algorithm kernel and parameter settings were selected for comparison to our PLS and OLS results. It is important to note again that SVM, RF

and PLS were not suitable for use with the hybrid and generalized hierarchical model-based (GHMB) estimators employed by the GEDI L4B gridded biomass product, but the objective here was to compare their general performance to the OLS models developed in this paper. Previous large area remote sensing studies have indicated that in reference to independent validation data, machine learning techniques such as SVM and RF, even when carefully parameterised, have not outperformed carefully specified OLS estimators such as those developed in this study (e.g. Armston et al., 2009), nor has PLS (Næsset et al., 2005).

Comparison of OLS, PLS, and Machine Learning Algorithms

The performance of the OLS results to the other three algorithms tested was similar across geographic strata. A comparison of these four modeling approaches is presented in Figs. S5 and S6 with square root transformed models fit within EBT PFT in Oceania. In this example, as in most of the other geographic strata, model performance was comparable between OLS, PLS, SVM and RF. In some geographic strata a particular algorithm type occasionally reduced the RMSE by a few percent, but OLS models performed comparably across the full range of strata explored. These results suggest that there was no clear advantage to using more complex algorithms, and that while machine learning approaches may indeed be more suitable for local applications when calibration datasets limit the utility of OLS (e.g., correlated predictors or nonlinear solutions), simple linear parametric models were similarly suitable for development of widely applicable models at a global scale. Additionally, as noted above, OLS was more transferable and less sensitive to the representativeness of training samples than machine learning approaches. Further, where more complex models are difficult to meaningfully interpret, simple parametric models facilitate an understanding of relationships between height and

structure, thus opening a pathway toward continual improvement and refinement of models as the community learns more about forest structure at a global scale.

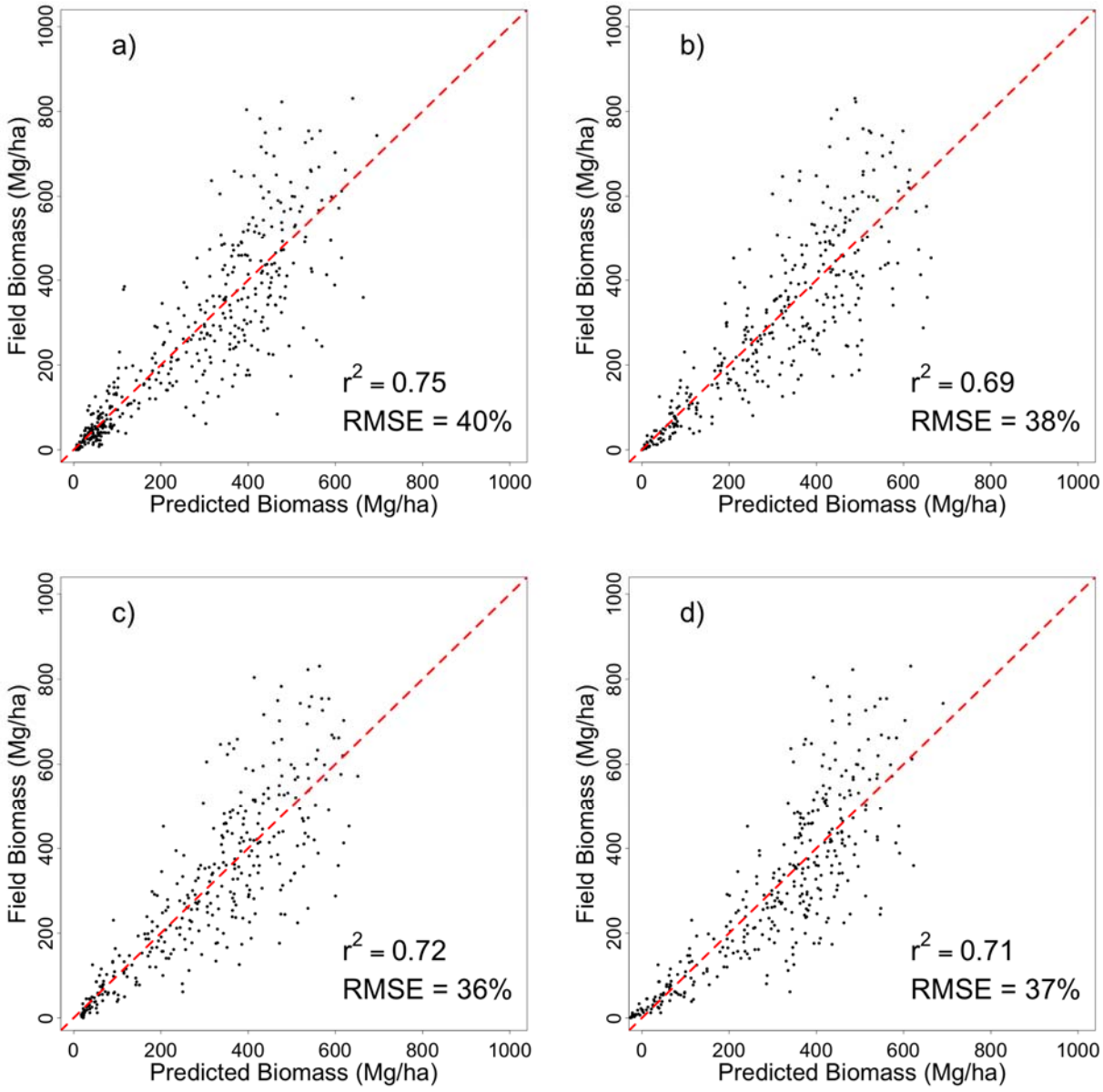

Fig S5 PFT by geographic region model fits in Evergreen Broadleaf Trees, Oceania using (a) OLS, b) RF, c) SVM and d) PLS).

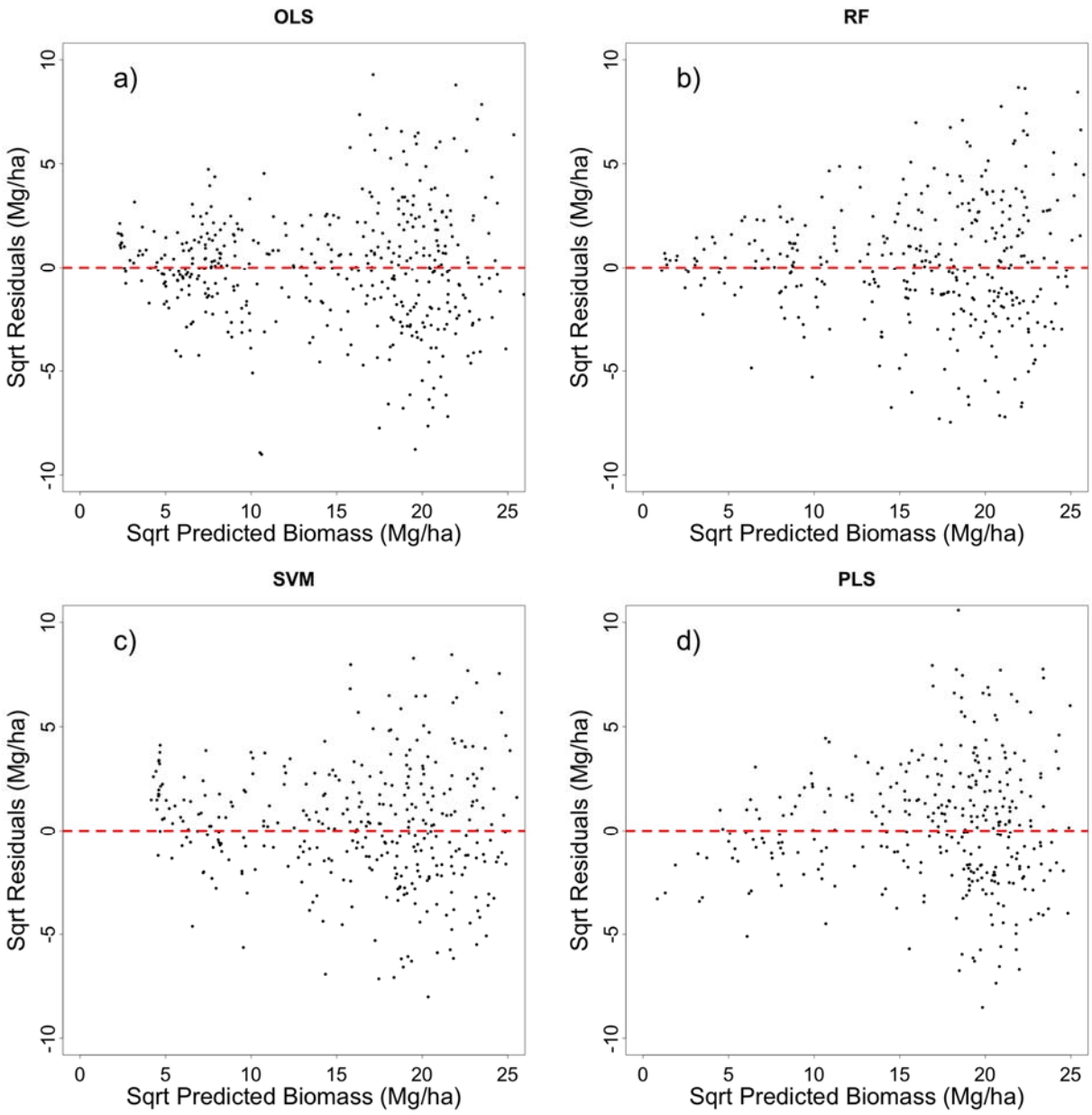

Fig. S6. PFT by geographic region residual plots for model fits in Evergreen Broadleaf Trees, Oceania using (a) OLS, b) RF, c) SVM and d) PLS).

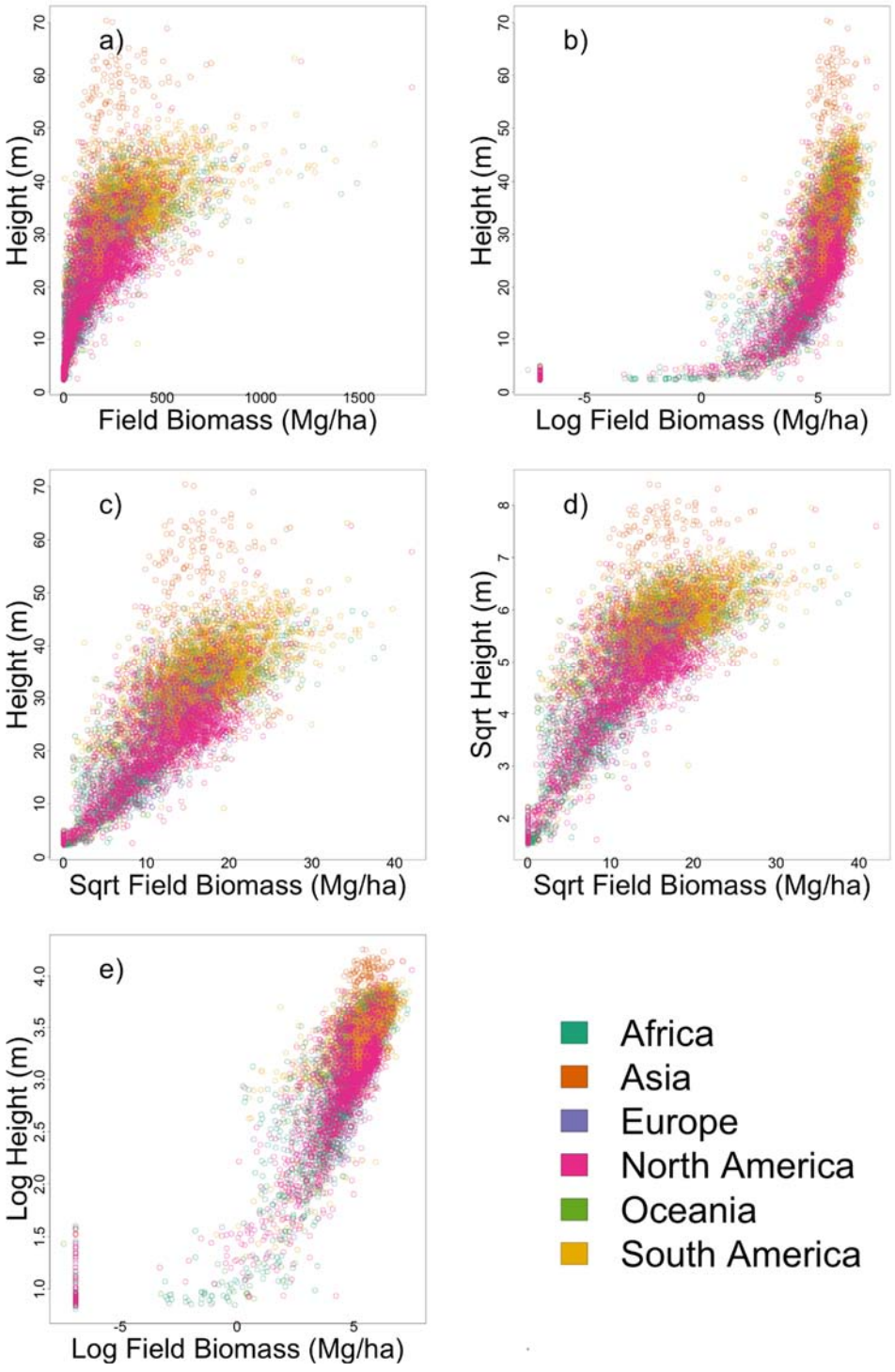

Fig. S7. Transformations affect the linearity between height metrics and field estimated AGBD. Here we show four different transformations, a) height (RH98 +100) vs biomass, b) height vs log transformed biomass, c) height vs square root transformed biomass, d) square root transformed

height against square root transformed biomass, and e) log transformed height against log transform.

References

Abdi, H., 2010. Partial least squares regression and projection on latent structure regression (PLS Regression). WIREs Computational Statistics. https://doi.org/10.1002/wics.51

Armston, J.D., Denham, R.J., Danaher, T.J., Scarth, P.F., Moffiet, T.N., 2009. Prediction and validation of foliage projective cover from Landsat-5 TM and Landsat-7 ETM imagery. Journal of Applied Remote Sensing 3, 033540.

Bastin, J.-F., Barbier, N., Couteron, P., Adams, B., Shapiro, A., Bogaert, J., De Cannière, C., 2014. Aboveground biomass mapping of African forest mosaics using canopy texture analysis: toward a regional approach. Ecol. Appl. 24, 1984–2001.

Beets, P.N., Kimberley, M.O., Oliver, G.R., Pearce, S.H., Doug Graham, J., Brandon, A., 2012. Allometric Equations for Estimating Carbon Stocks in Natural Forest in New Zealand. Forests. https://doi.org/10.3390/f3030818

Boyd, D.S., Hill, R.A., Hopkinson, C., Baker, T.R., 2013. Landscape-scale forest disturbance regimes in southern Peruvian Amazonia. Ecol. Appl. 23, 1588–1602.

Bradford, M.G., Metcalfe, D.J., Ford, A., Liddell, M.J., McKeown, A., 2014. Floristics, stand structure and aboveground biomass of a 25-ha rainforest plot in the wet tropics of Australia. J. Trop. For. Sci. 26, 543–553.

Breiman, L., 2001. Random forests. Mach. Learn. 45, 5–32.

Brown, C., Boyd, D.S., Sjögersten, S., Clewley, D., Evers, S.L., Aplin, P., 2018. Tropical peatland vegetation structure and biomass: Optimal exploitation of airborne laser scanning. Remote Sensing 10, 671.

Calvo-Rodriguez, S., Sánchez-Azofeifa, G.A., Durán, S.M., Do Espírito-Santo, M.M., Nunes, Y.R.F., 2021. Dynamics of Carbon Accumulation in Tropical Dry Forests under Climate Change Extremes. For. Trees Livelihoods 12, 106.

Chave, J., Andalo, C., Brown, S., Cairns, M.A., Chambers, J.Q., Eamus, D., Fölster, H., Fromard, F., Higuchi, N., Kira, T., Lescure, J.-P., Nelson, B.W., Ogawa, H., Puig, H., Riéra, B., Yamakura, T., 2005. Tree allometry and improved estimation of carbon stocks and balance in tropical forests. Oecologia 145, 87–99.

Chave, J., Réjou-Méchain, M., Búrquez, A., Chidumayo, E., Colgan, M.S., Delitti, W.B.C., Duque, A., Eid, T., Fearnside, P.M., Goodman, R.C., Henry, M., Martínez-Yrízar, A., Mugasha, W.A., Muller-Landau, H.C., Mencuccini, M., Nelson, B.W., Ngomanda, A., Nogueira, E.M., Ortiz-Malavassi, E., Pélissier, R., Ploton, P., Ryan, C.M., Saldarriaga, J.G., Vieilledent, G., 2014. Improved allometric models to estimate the aboveground biomass of tropical trees. Glob. Chang. Biol. 20, 3177–3190.

Clark, M.L., Roberts, D.A., Ewel, J.J., Clark, D.B., 2011. Estimation of tropical rain forest aboveground biomass with small-footprint lidar and hyperspectral sensors. Remote Sens.

Environ. 115, 2931–2942.
Colgan, M.S., Asner, G.P., Swemmer, T., 2013. Harvesting tree biomass at the stand level to assess the accuracy of field and airborne biomass estimation in savannas. Ecol. Appl. 23, 1170–1184.
Condit, R., Pérez, R., Aguilar, S., Lao, S., Foster, R., Hubbell, S., 2019. Complete data from the Barro Colorado 50-ha plot: 423617 trees, 35 years, 2019 version. https://doi.org/10.15146/5xcp-0d46
Condit, R., Pérez, R., Aguilar, S., Lao, S., Foster, R., Stephen, H., 2020. BCI 50-ha Plot Taxonomy, 2019 version. https://doi.org/10.15146/R3FH61
Corona, P., Fattorini, L., Franceschi, S., Scrinzi, G., Torresan, C., 2014. Estimation of standing wood volume in forest compartments by exploiting airborne laser scanning information: model-based, design-based, and hybrid perspectives. Can. J. For. Res. 44, 1303–1311.
Dalponte, M., Coomes, D.A., 2016. Tree-centric mapping of forest carbon density from airborne laser scanning and hyperspectral data. Methods Ecol. Evol. 7, 1236–1245.
de Almeida, D.R.A., Zambrano, A.M.A., Broadbent, E.N., Wendt, A.L., Foster, P., Wilkinson, B.E., Salk, C., Papa, D. de A., Stark, S.C., Valbuena, R., Gorgens, E.B., Fagan, Carlos Alberto Silva14,15 | Pedro Henrique Santin Brancalion1 | Matthew, Meli, P., Chazdon, R., 2020. Detecting successional changes in tropical forest structure using GatorEye drone-borne lidar. Biotropica 00, 1–13.
Demaerschalk, J.P., Kozak, A., 1974. Suggestions and criteria for more effective regression sampling. Can. J. For. Res. 4, 341–348.
Deng, S., Katoh, M., Yu, X., Hyyppä, J., Gao, T., 2016. Comparison of Tree Species Classifications at the Individual Tree Level by Combining ALS Data and RGB Images Using Different Algorithms. Remote Sensing. https://doi.org/10.3390/rs8121034
Drucker, H., Burges, C.J., Kaufman, L., Smola, A., Vapnik, V., 1996. Support vector regression machines. Adv. Neural Inf. Process. Syst. 9, 155–161.
Dubayah, R.O., Sheldon, S.L., Clark, D.B., Hofton, M.A., Blair, J.B., Hurtt, G.C., Chazdon, R.L., 2010. Estimation of tropical forest height and biomass dynamics using lidar remote sensing at La Selva, Costa Rica. Journal of Geophysical Research: Biogeosciences. https://doi.org/10.1029/2009jg000933
Dubayah, R.O., Swatantran, A., Huang, W., Duncanson, L., Tang, H., Johnson, K., Dunne, J.O., Hurtt, G.C., 2017. CMS: LiDAR-derived Biomass, Canopy Height and Cover, Sonoma County, California, 2013. ORNL DAAC, Oak Ridge, Tennessee, USA.
Duncanson, L., Dubayah, R.O., Armston, J., Liang, M., Arthur, A., Minor, D., 2020. CMS: LiDAR Biomass Improved for High Biomass Forests, Sonoma County, CA, USA, 2013. ORNL DAAC.
Duncanson, L., Huang, W., Johnson, K., Swatantran, A., McRoberts, R.E., Dubayah, R., 2017. Implications of allometric model selection for county-level biomass mapping. Carbon Balance Manag. 12, 18.
Duncanson, L.I., Dubayah, R.O., Cook, B.D., Rosette, J., Parker, G., 2015. The importance of

spatial detail: Assessing the utility of individual crown information and scaling approaches for lidar-based biomass density estimation. Remote Sensing of Environment. https://doi.org/10.1016/j.rse.2015.06.021

Duque, A., Saldarriaga, J., Meyer, V., Saatchi, S., 2017. Structure and allometry in tropical forests of Chocó, Colombia. For. Ecol. Manage. 405, 309–318.

Ellis, P., Griscom, B., Walker, W., Gonçalves, F., Cormier, T., 2016. Mapping selective logging impacts in Borneo with GPS and airborne lidar. Forest Ecology and Management. https://doi.org/10.1016/j.foreco.2016.01.020

Ene, L.T., Næsset, E., Gobakken, T., Martin Bollandsås, O., Mauya, E.W., Zahabu, E., 2017. Large-scale estimation of change in aboveground biomass in miombo woodlands using airborne laser scanning and national forest inventory data. Remote Sens. Environ. 188, 106–117.

Fekety, P.A., Hudak, A.T., Bright, B.C., 2020. Field observations for "A carbon monitoring system for mapping regional, annual aboveground biomass across the northwestern USA." https://doi.org/10.2737/RDS-2020-0026

Fernández-Landa, A., 2015. LiDAR remote sensing applied to forest resources assessment (Doctoral dissertation). Universidad Politécnica de Madrid.

Ferraz, A., Saatchi, S., Xu, L., Hagen, S., Chave, J., Yu, Y., Meyer, V., Garcia, M., Silva, C., Roswintiart, O., Samboko, A., Sist, P., Walker, S., Pearson, T.R.H., Wijaya, A., Sullivan, F.B., Rutishauser, E., Hoekman, D., Ganguly, S., 2018. Carbon storage potential in degraded forests of Kalimantan, Indonesia. Environ. Res. Lett. 13, 095001.

Forrester, D.I., Tachauer, I.H.H., Annighoefer, P., Barbeito, I., Pretzsch, H., Ruiz-Peinado, R., Stark, H., Vacchiano, G., Zlatanov, T., Chakraborty, T., Saha, S., Sileshi, G.W., 2017. Generalized biomass and leaf area allometric equations for European tree species incorporating stand structure, tree age and climate. Forest Ecology and Management. https://doi.org/10.1016/j.foreco.2017.04.011

Hansen, E.H., Gobakken Terje Bollandsås, Zahabu, E., Næsset, E., 2015. Modeling Aboveground Biomass in Dense Tropical Submontane Rainforest Using Airborne Laser Scanner Data. Remote Sensing 7, 788–807.

Huang, W., Sun, G., Dubayah, R., Cook, B., Montesano, P., Ni, W., Zhang, Z., 2013. Mapping biomass change after forest disturbance: Applying LiDAR footprint-derived models at key map scales. Remote Sensing of Environment. https://doi.org/10.1016/j.rse.2013.03.017

Janík, D., Král, K., Adam, D., Hort, L., Samonil, P., Unar, P., Vrska, T., McMahon, S., 2016. Tree spatial patterns of Fagus sylvatica expansion over 37 years. For. Ecol. Manage. 375, 134–145.

Jenkins, J.C., Chojnacky, D.C., Heath, L.S., Birdsey, R.A., 2003. National-scale biomass estimators for United States tree species. For. Sci. 49, 12–35.

Jensen, J.L.R., Humes, K.S., Vierling, L.A., Hudak, A.T., 2008. Discrete return lidar-based prediction of leaf area index in two conifer forests. Remote Sens. Environ. 112, 3947–

3957.
Jucker, T., Bongalov, B., Burslem, D.F.R.P., Nilus, R., Dalponte, M., Lewis, S.L., Phillips, O.L., Qie, L., Coomes, D.A., 2018. Topography shapes the structure, composition and function of tropical forest landscapes. Ecol. Lett. 21, 989–1000.
Kearsley, E., de Haulleville, T., Hufkens, K., Kidimbu, A., Toirambe, B., Baert, G., Huygens, D., Kebede, Y., Defourny, P., Bogaert, J., Beeckman, H., Steppe, K., Boeckx, P., Verbeeck, H., 2013. Conventional tree height-diameter relationships significantly overestimate aboveground carbon stocks in the Central Congo Basin. Nat. Commun. 4, 2269.
Kellner, J.R., Armston, J., Birrer, M., Cushman, K.C., Duncanson, L., Eck, C., Falleger, C., Imbach, B., Král, K., Krůček, M., Trochta, J., Vrška, T., Zgraggen, C., 2019. New Opportunities for Forest Remote Sensing Through Ultra-High-Density Drone Lidar. Surv. Geophys. 40, 959–977.
Knapp, N., Fischer, R., Cazcarra-Bes, V., Huth, A., 2020. Structure metrics to generalize biomass estimation from lidar across forest types from different continents. Remote Sens. Environ. 237, 111597.
Krause, K., Goulden, T., 2015. NEON.DOC.001292: NEON L0-TO-L1 DISCRETE RETURN LiDAR ALGORITHM THEORETICAL BASIS DOCUMENT (ATBD). NEON.
Krůček, M., Kc, K.K.C., Missarov, A., Kellner, J.R., 2020. Supervised Segmentation of Ultra-High-Density Drone Lidar for Large-Area Mapping of Individual Trees. Remote Sensing 12, 3260.
Krzystek, P., Serebryanyk, A., Schnörr, C., Červenka, J., Heurich, M., 2020. Large-Scale Mapping of Tree Species and Dead Trees in Šumava National Park and Bavarian Forest National Park Using Lidar and Multispectral Imagery. Remote Sensing. https://doi.org/10.3390/rs12040661
Kükenbrink, D., Schneider, F.D., Leiterer, R., Schaepman, M.E., Morsdorf, F., 2017. Quantification of hidden canopy volume of airborne laser scanning data using a voxel traversal algorithm. Remote Sensing of Environment. https://doi.org/10.1016/j.rse.2016.10.023
Labriere, N., Tao, S., Chave, J., Scipal, K., Le Toan, T., Abernethy, K., Alonso, A., Barbier, N., Bissiengou, P., Casal, T., Davies, S.J., Ferraz, A., Herault, B., Jaouen, G., Jeffery, K.J., Kenfack, D., Korte, L., Lewis, S.L., Malhi, Y., Memiaghe, H.R., Poulsen, J.R., Rejou-Mechain, M., Villard, L., Vincent, G., White, L.J.T., Saatchi, S., 2018. In Situ Reference Datasets From the TropiSAR and AfriSAR Campaigns in Support of Upcoming Spaceborne Biomass Missions. IEEE Journal of Selected Topics in Applied Earth Observations and Remote Sensing. https://doi.org/10.1109/jstars.2018.2851606
Lambert, M.-C., Ung, C.-H., Raulier, F., 2005. Canadian national tree aboveground biomass equations. Canadian Journal of Forest Research. https://doi.org/10.1139/x05-112
Lang, M., Arumäe, T., Laarmann, D., Kiviste, A., 2017. Estimation of change in forest height growth. For. Stud. China 67, 5–16.

Latifi, H., Fassnacht, F.E., Müller, J., Tharani, A., Dech, S., Heurich, M., 2015. Forest inventories by LiDAR data: A comparison of single tree segmentation and metric-based methods for inventories of a heterogeneous temperate forest. International Journal of Applied Earth Observation and Geoinformation. https://doi.org/10.1016/j.jag.2015.06.008

Legner, K., Andersen, H.-E., Cooke, A., Cohen, W., 2020. A Cost-effective Field Measurement Protocol to Support Lidar-assisted Carbon Monitoring Programs: Implementing a Prototype Design at Six Different Sites in the United States, General Technical Report (GTR). U.S. Department of Agriculture, Forest Service, Pacific Northwest Research Station., Portland, OR.

Lobo, E., Dalling, J.W., 2014. Spatial scale and sampling resolution affect measures of gap disturbance in a lowland tropical forest: implications for understanding forest regeneration and carbon storage. Proceedings of the Royal Society B 281. https://doi.org/10.1098/rspb.2013.3218

Longo, M., Keller, M., dos-Santos, M.N., Leitold, V., Pinagé, E.R., Baccini, A., Saatchi, S., Nogueira, E.M., Batistella, M., Morton, D.C., 2016. Aboveground biomass variability across intact and degraded forests in the Brazilian Amazon. Global Biogeochem. Cycles 30, 1639–1660.

Los, S.O., Rosette, J.A.B., Kljun, N., North, P.R.J., Chasmer, L., Suárez, J.C., Hopkinson, C., Hill, R.A., van Gorsel, E., Mahoney, C., Berni, J.A.J., 2012. Vegetation Height and Cover Fraction Between 60° S and 60° N from ICESat GLAS Data. Geoscientific Model Development 5, 413–432.

Masota, A.M., Bollandsås, O.M., Zahabu, E., Eid, T., 2016. Allometric biomass and volume models for lowland and humid montane forests, in: Malimbwi, R.E., Eid, T., Chamshama, S.A.O. (Eds.), Allometric Tree Biomass and Volume Models in Tanzania. Department of forest mensuration and management, Sokoine University of Agriculture, Morogoro, Tanzania, pp. 35–46.

Meier, C., Jones, K., 2020. NEON.DOC.000987: TOS PROTOCOL AND PROCEDURE: VST – MEASUREMENT OF VEGETATION STRUCTURE. NEON.

Mevik, B.-H., Wehrens, R., 2007. The pls Package: Principal Component and Partial Least Squares Regression inR. Journal of Statistical Software. https://doi.org/10.18637/jss.v018.i02

Meyer, D., 2020. Support vector machines.

Meyer, V., Saatchi, S., Ferraz, A., Xu, L., Duque, A., García, M., Chave, J., 2019. Forest degradation and biomass loss along the Chocó region of Colombia. Carbon Balance Manag. 14, 2.

Montesano, P.M., Cook, B.D., Sun, G., Simard, M., Nelson, R.F., Ranson, K.J., Zhang, Z., Luthcke, S., 2013. Achieving accuracy requirements for forest biomass mapping: A spaceborne data fusion method for estimating forest biomass and LiDAR sampling error. Remote Sens. Environ. 130, 153–170.

Moore, J.R., 2010. Allometric equations to predict the total above-ground biomass of radiata pine trees. Annals of Forest Science. https://doi.org/10.1051/forest/2010042

Mugasha, W.A., Eid, T., Bollandsås, O.M., Malimbwi, R.E., Chamshama, S.A.O., Zahabu, E., Katani, J.Z., 2013. Allometric models for prediction of above- and belowground biomass of trees in the miombo woodlands of Tanzania. Forest Ecology and Management. https://doi.org/10.1016/j.foreco.2013.08.003

Muukkonen, P., 2007. Generalized allometric volume and biomass equations for some tree species in Europe. European Journal of Forest Research. https://doi.org/10.1007/s10342-007-0168-4

Næsset, E., Bollandsås, O.M., Gobakken, T., 2005. Comparing regression methods in estimation of biophysical properties of forest stands from two different inventories using laser scanner data. Remote Sens. Environ. 94, 541–553.

Naidoo, L., Mathieu, R., Main, R., Kleynhans, W., Wessels, K., Asner, G., Leblon, B., 2015. Savannah woody structure modelling and mapping using multi-frequency (X-, C- and L-band) Synthetic Aperture Radar data. ISPRS J. Photogramm. Remote Sens. 105, 234–250.

Orwig, D.A., Aylward, J.A., Buckley, H.L., Case, B.S., Ellison, A.M., 2021 Land-use history impacts spatial patterns and composition of woody plant species across a 35-hectare temperate forest plot. bioRxiv. https://doi.org/10.1101/2021.04.07.438791

Orwig, D., Foster, D., Ellison, A., 2015. Harvard Forest CTFS-ForestGEO Mapped Forest Plot since 2014.

Panciera, R., Walker, J.P., Jackson, T.J., Gray, D.A., Tanase, M.A., Ryu, D., Monerris, A., Yardley, H., Rudiger, C., Wu, X., Gao, Y., Hacker, J.M., 2014. The Soil Moisture Active Passive Experiments (SMAPEx): Toward Soil Moisture Retrieval From the SMAP Mission. IEEE Transactions on Geoscience and Remote Sensing. https://doi.org/10.1109/tgrs.2013.2241774

Paul, K.I., Roxburgh, S.H., Chave, J., England, J.R., Zerihun, A., Specht, A., Lewis, T., Bennett, L.T., Baker, T.G., Adams, M.A., Huxtable, D., Montagu, K.D., Falster, D.S., Feller, M., Sochacki, S., Ritson, P., Bastin, G., Bartle, J., Wildy, D., Hobbs, T., Larmour, J., Waterworth, R., Stewart, H.T.L., Jonson, J., Forrester, D.I., Applegate, G., Mendham, D., Bradford, M., O'Grady, A., Green, D., Sudmeyer, R., Rance, S.J., Turner, J., Barton, C., Wenk, E.H., Grove, T., Attiwill, P.M., Pinkard, E., Butler, D., Brooksbank, K., Spencer, B., Snowdon, P., O'Brien, N., Battaglia, M., Cameron, D.M., Hamilton, S., McAuthur, G., Sinclair, J., 2016. Testing the generality of above-ground biomass allometry across plant functional types at the continent scale. Glob. Chang. Biol. 22, 2106–2124.

Philipson, C.D., Cutler, M.E.J., Brodrick, P.G., Asner, G.P., Boyd, D.S., Costa, P.M., Fiddes, J., Foody, G.M., van der Heijden, G.M.F., Ledo, A., Lincoln, P.R., Margrove, J.A., Martin, R.E., Milne, S., Pinard, M.A., Reynolds, G., Snoep, M., Tangki, H., Wai, Y.S., Wheeler, C.E., David F R, 2020. Active restoration accelerates the carbon recovery of human-modified tropical forests. Science 369, 838–841.

Sanchez-Lopez, N., Boschetti, L., Hudak, A.T., 2020a. Reconstruction of the disturbance history of a temperate coniferous forest through stand-level analysis of airborne LiDAR data. Forestry: An International Journal of Forest Research 93, 38–55.

Sanchez-Lopez, N., Boschetti, L., Hudak, A.T., Hancock, S., Duncanson, L.I., 2020b. Estimating Time Since the Last Stand-Replacing Disturbance (TSD) from Spaceborne Simulated GEDI Data: A Feasibility Study. Remote Sensing 12, 3506.

Schneider, F.D., Morsdorf, F., Schmid, B., Petchey, O.L., Hueni, A., Schimel, D.S., Schaepman, M.E., 2017. Mapping functional diversity from remotely sensed morphological and physiological forest traits. Nat. Commun. 8, 1441.

Simard, M., Denbina, M., 2018. An assessment of temporal decorrelation compensation methods for forest canopy height estimation using airborne L-band same-day repeat-pass polarimetric SAR interferometry. IEEE Journal of Selected Topics in Applied Earth Observations and Remote Sensing 11, 95–111.

Stereńczak, K., Kraszewski, B., Mielcarek, M., Piasecka, Ż., 2017. Inventory of standing dead trees in the surroundings of communication routes – The contribution of remote sensing to potential risk assessments. For. Ecol. Manage. 402, 76–91.

Stereńczak, K., Mielcarek, M., Modzelewska, A., Kraszewski, B., Fassnacht, F.E., Hilszczański, J., 2019. Intra-annual Ips typographus outbreak monitoring using a multi-temporal GIS analysis based on hyperspectral and ALS data in the Białowieża Forests. For. Ecol. Manage. 442, 105–116.

Sumnall, M.J., Hill, R.A.H., Hinsley, S.A., 2016. Comparison of small-footprint discrete return and full waveform airborne lidar data for estimating multiple forest variables. Remote Sens. Environ. 173, 214–223.

Valbuena, R., Mauro, F., Rodríguez-Solano, R., Manzanera, J.A., 2012. Partial Least Squares for Discriminating Variance Components in Global Navigation Satellite Systems Accuracy Obtained Under Scots Pine Canopies. For. Sci. 58, 139–153.

Valbuena, R., Packalén, P., Martı´n-Fernández, S., Maltamo, M., 2012. Diversity and equitability ordering profiles applied to study forest structure. Forest Ecology and Management 276, 185–195.

Valbuena, R., Packalen, P., Mehtätalo, L., García-Abril, A., Maltamo, M., 2013. Characterizing forest structural types and shelterwood dynamics from Lorenz-based indicators predicted by airborne laser scanning. Can. J. For. Res. 43, 1063–1074.

White, J.C., Chen, H., Woods, M.E., Low, B., Nasanova, S., 2019. The Petawawa Research Forest: Establishment of a remote sensing supersite. For. Chron. 95, 149–156.

Wood, S.W., Prior, L.D., Stephens, H.C., Bowman, D.M.J.S., 2015. Macroecology of Australian Tall Eucalypt Forests: Baseline Data from a Continental-Scale Permanent Plot Network. PLoS One 10, e0137811.